International Journal of Nanomedicine

Dovepress
open access to scientific and medical research

Open Access Full Text Article

ORIGINAL RESEARCH

Preclinical evaluation of recombinant human IFNα_2b-containing magnetoliposomes for treating hepatocellular carcinoma

This article was published in the following Dove Press journal:
International Journal of Nanomedicine
25 September 2014
Number of times this article has been viewed

Hui Ye[1,2]
Jiansong Tong[2]
Jianzhang Wu[3]
Xia Xu[4]
Shenjie Wu[5]
Botao Tan[6]
Mengjing Shi[5]
Jianguang Wang[1]
Weibo Zhao[5]
Heng Jiang[5]
Sha Jin[5]

[1]School of Basic Medical Sciences, Wenzhou Medical University, Wenzhou, People's Republic of China; [2]Department of Cellular and Molecular Biology, Scripps Research Institute, La Jolla, CA, USA; [3]Pharmaceutical College, Wenzhou Medical University, Wenzhou, [4]School of Medicine, Zhejiang University, Hangzhou, [5]School of the 1st Clinical Medical Sciences, Wenzhou Medical University, Wenzhou, [6]School of Medicine, Lishui University, Lishui, People's Republic of China

Correspondence: Hui Ye
School of Basic Medical Sciences, Wenzhou Medical University, Ouhai, Wenzhou, Zhejiang 325035, People's Republic of China
Email huiye1109@gmail.com

Abstract: Magnetoliposomes are phospholipid vesicles encapsulating magnetic nanoparticles that can be used to encapsulate therapeutic drugs for delivery into specific organs. Herein, we developed magnetoliposomes containing recombinant human IFNα_2b, designated as MIL, and evaluated this combination's biological safety and therapeutic effect on both cellular and animal hepatocellular carcinoma models. Our data showed that MIL neither hemolyzed erythrocytes nor affected platelet-aggregation rates in blood. Nitroblue tetrazolium-reducing testing showed that MIL did not change the absolute numbers or phagocytic activities of leukocytes. Acute-toxicity testing also showed that MIL had no devastating effect on mice behaviors. All the results indicated that the nanoparticles could be a safe biomaterial. Pharmacokinetic analysis and tissue-distribution studies showed that MIL maintained stable and sustained drug concentrations in target organs under a magnetic field, helped to increase bioavailability, and reduced administration time. MIL also dramatically inhibited the growth of hepatoma cells. Targeting of MIL in the livers of nude mice bearing human hepatocellular carcinoma showed that MIL significantly reduced the tumor size to 38% of that of the control group. Further studies proved that growth inhibition of cells or tumors was due to apoptosis-signaling pathway activation by human IFNα_2b.

Keywords: recombinant human interferon-α_2b, magnetoliposome, hepatocellular carcinoma

Introduction

Hepatocellular carcinoma (HCC) is the third-leading cause of death and the fifth-most common malignancy worldwide.[1,2] Currently, liver transplantation is the best treatment option for most HCC patients.[3] Drug treatment, especially recent developments in targeted drugs with various therapeutic agents, has also been recommended as an excellent therapeutic strategy.[4] IFN has been suggested to play an important role in antivirus, antiproliferative, and immunoregulatory pathways.[5–7] Some studies show that IFNα, including IFNα_2b, is also capable of exerting antitumor effects against HCC, hairy cell leukemia, lymphoma, melanoma, and breast cancer.[3,8–16] However, an extensive clinical trial of IFNα_2b for HCC was delayed, due to the weak therapeutic effect based on conventional drug-delivery methods. In general, these methods cause rapid degradation of IFNα_2b in the body and induce severe side effects, due to the systemic distribution of drugs in the body causing bone marrow suppressions and neurologic disorders.[15]

Conventional targeting and drug-delivery methods for HCC are limited to common liposomes, nanoparticles (NPs), and intravenous emulsions.[15,17–19] Therefore, the surge of interest in this field has greatly expanded the extent of research on magnetic NPs

(MNPs). Some of the most promising applications of biologically inspired NPs have so far been applied to nanobiotechnology and specific drug delivery. MNPs have been proposed as drug-delivery systems to enhance drug delivery to cancer cells based on their ability to target specific locations. The magnetic properties can cause the drugs to be retained in a location under a magnetic field. Currently, MNPs of iron oxide, which are easy to produce, easy to functionalize, and present satisfactory water solubility and slow degradation in vivo, have been reported as promising biocompatible materials in the anticancer field.[20–23]

Magnetic materials with a biodegradable carrier (liposomes) have been conceived as a new formulation method for targeted drug-delivery systems.[24] Liposomes have excellent half-life periods, and can be gradually biodegraded in the body. In addition, anticancer drugs remaining in the target area under an external magnetic field are slowly released and directed toward target tissues.[20,24] This type of system can significantly improve the efficiency of anticancer drugs and decrease side effects caused by systemic distribution of the drugs in the body.

In the present study, we developed a novel magnetoliposome (ML) containing recombinant human (rh)-IFNα_2b (MIL), and demonstrated it as a safe biomaterial through hemolysis and acute-toxicity tests. MIL can maintain stable and sustained blood drug concentrations, especially under the guidance of a magnetic field, which increases the bioavailability of the material and reduces its administration times. Finally, we evaluated the effect of MIL on cell-growth inhibition and tumor-size reduction on a human cancer model using nude mice.

Materials and methods

Cells and animals

Bel-7402 cells were purchased from the American Type Culture Collection (ATCC; USA) and cultured in Roswell Park Memorial Institute (RPMI) 1640 medium (Invitrogen, USA) containing 10% fetal bovine serum (Sigma, USA), 100 U/mL penicillin, and 50 μg/mL streptomycin in 20 cm^2 tissue-culture flasks (Falcon, USA). Cells were maintained at 37°C in humidified incubators with 5% CO_2 and passaged every 3 days.

New Zealand rabbits (weight 1.8–2.5 kg), imprinting control region (ICR) mice (weight 18–22 g, males and females of equal number) and Sprague Dawley rats (weight 180–200 g) were purchased from the Shanghai Laboratory Animal Center, Chinese Academy of Sciences, People's Republic of China (PRC). Six-week-old nude male BALB/c mice (weight 18–20 g; Shanghai Laboratory Animal Center) were housed in laminar flow cabinets under specific pathogen-free conditions and provided with water and food ad libitum. All animals were cared for and handled according to the recommendations of the National Institutes of Health's *Guide for the Care and Use of Laboratory Animals*. Animal protocols were approved by the Shanghai Medical Experimental Animal Care Committee.

Chemicals and reagents

Dimyristoyl phosphatidyl glycerol (DMPG), egg-yolk phosphatidylcholine (PC), cholesterol (Chol), chloroform, and Triton X-100 were purchased from Sigma. Sephadex G-50 was purchased from Pharmacia Fine Chemicals (Uppsala, Sweden). rhIFNα_2b and rhIFNα_2b "sandwich" enzyme-linked immunosorbent assay (ELISA) kits were purchased from Schering Canada. Ultrafine magnetite (Fe_3O_4, mean diameter 10 nm) was received from the Southwest Institute of Applied Magnetics of China (PRC). MTT (3-[4,5-dimethylthiazol-2-yl]-2,5-diphenyltetrazolium bromide) cell-proliferation assay kits were purchased from ATCC. Acridine orange solution was purchased from Sigma. Trizol reagent, deoxyribonuclease I enzyme, SuperScript® III reverse transcriptase and AccuPrime™ Pfx deoxyribonucleic acid (DNA) polymerase were purchased from Invitrogen (USA). BCA protein assay kits were purchased from Pierce (USA). Polyvinylidene difluoride membranes were purchased from Bio-Rad Laboratories (USA). Polyclonal antibodies of rabbit antihuman Bcl-2, Bax, and β-actin were purchased from Santa Cruz Biotech (USA). Horseradish peroxidase-conjugated goat antirabbit IgG and electrochemiluminescence kits were purchased from Amersham Pharmacia Biotech (USA). All other reagents and solvents used were analytical grade.

MIL preparation and purification

The MIL was prepared by reverse-phase evaporation combined with ice-water bath ultrasonication. Briefly, different molar ratios of egg-yolk PC, Chol, and DMPG were dissolved in an appropriate volume of chloroform. The mixture was dried to a thin lipid film on the wall of a round-bottom flask in a rotary flash evaporator (Büchi, Switzerland) under reduced pressure at 40°C±0.5°C and 150 rpm/min. The lipid film obtained was introduced with 3 mL of phosphate-buffered saline (PBS) containing rhIFNα_2b (400×10^4 IU) and ultrafine magnetite (10 nm Fe_3O_4, 50 mg) and then placed in an ice-water bath ultrasonicator until a single-phase liquid formed. The liquid was then evaporated under high-vacuum conditions to form a viscous gel that subsequently became a water-like suspension. Evaporation was continued for 15 minutes

to remove all traces of the solvent. The resulting suspension was flushed with nitrogen, sealed, and placed in an ice-water bath ultrasonicator for 20–60 minutes. Afterward, the MIL was separated from free rhIFNα$_2$b and ferrofluid particles by column chromatography on Sephadex G-50 minicolumns saturated with lipids before sample elution, and the eluent was further distilled. rhIFNα$_2$b liposomes (ILs) were prepared by the same method, but without addition of ultrafine magnetite.

The purified MIL, IL, and ML were sterilized by the 0.39 kGy radiation with ^{60}Co-γ rays. The particle size and encapsulation efficiency of different liposomes were compared before and after irradiation.

Morphology and biophysical characterization of MIL

The morphology of magnetite and MIL was examined by a JEM-100cx (JEOL, Japan) transmission electron microscope operating at 80 kV. Briefly, a drop of the diluted magnetite or MIL was mounted on a 400-mesh copper grid coated with carbon film. Before analysis, samples were stained with uranyl acetate and allowed to dry at room temperature. Micrographs were recorded with a MegaView III camera. Acquisition was accomplished using Soft Imaging software (Germany).

The mean size and size distribution of the particles were determined by dynamic light scattering (DLS) at 25°C with a scattering angle of 90° using a Zetasizer Nano instrument (Malvern Instruments, UK). The particle suspension was diluted with Tris buffer for analysis. To measure the distribution of particle sizes in the dispersion, the polydispersity index (PI) was calculated. The number-average diameter (d) and size distribution (coefficient of variation [CV]) were defined as follows:

$$d=\sum_{i=1}^{n}\frac{d}{N},\ CV=\left[\sum_{i=1}^{n}\frac{(di-d)^2}{N}\right]^{1/2}\sqrt{d}, \qquad (1)$$

here, di is the diameter of each particle, and N is the total number of measured particles. All values were measured in triplicate, and the results are shown as mean standard distributions.

ELISA assay

ELISA assays were performed to determine the rhIFNα$_2$b-encapsulation efficiency of MIL and IL. Briefly, a 96-well plate was coated with 2 μg/mL of antihuman IFNα$_2$b monoclonal antibody in coating buffer (0.1 M sodium carbonate, pH 9.6) at 4°C for 24–48 hours. The plate was washed three times with washing buffer (0.01 M PBS, 0.02% Tween 20, pH 7.4). Around 100 μL of a sample containing IFNα$_2$b was added to each well. Various concentrations (5, 2.5, 1.25, 0.625, 0.312, 0.156, and 0.078 ng/mL) of free IFNα$_2$b were used to prepare a standard curve. The plate was incubated at 37°C for 1 hour and washed three times with washing buffer, followed by the addition of 100 μL of horseradish peroxidase-conjugated goat antihuman IFNα$_2$b antibody at a final dilution of 1:2,000 into each well and incubation at 37°C for 45 minutes. After being washed five times to remove unbound antibodies, the plate was incubated with substrate solution (5.5 mg/mL of *o*-phenylenediamine, 5.5 μL/mL of H_2O_2 in PBS) at 37°C for 15–30 minutes. The reaction was stopped by the addition of 50 μL of 21% (w/v) H_2SO_4. Optical density (OD) was then read at 490 nm. The concentration of IFNα$_2$b in each sample was determined according to the derived standard curve based on the OD obtained. Drug-encapsulation efficiency was determined using the following equation:

$$\text{Encapsulation efficiency (\%)}=\frac{C_2}{C_1}\times 100, \qquad (2)$$

here, C_2 is the amount of rhIFNα$_2$b in MIL or IL, and C_1 is the total amount of rhIFNα$_2$b in the solution before chromatography.

Hemolytic tests

In vitro hemolytic tests were performed to determine the biological safety of MIL to red blood cells. Briefly, about 20 mL fresh rabbit blood was stirred with a glass rod to remove fibrinogen. About 100 mL of saline was then added to the blood, which was subsequently shaken and centrifuged (1,500 rpm) for 20 minutes to remove the supernatant. Pellets were further washed with saline several times until red coloration was no longer observed. The erythrocytes were collected and diluted with saline to obtain a 2% erythrocyte suspension. Eight tubes preheated at 37°C were filled with 5 mL of 2% rabbit erythrocyte suspension. Purified MIL (10,000 IU/mL rhIFNα$_2$b) at volumes of 0.1, 0.2, 0.3, 0.4, 0.5, or 0.6 mL was added to the first six tubes. Saline was added to these tubes to yield 10 mL solutions. The seventh tube was directly filled with 5 mL of saline as a negative control (no hemolysis), while the eighth tube was filled with 5 mL of double-distilled water as a positive control (100% hemolysis). After mixing, all tubes were incubated in a water bath at 37°C for 60 minutes and centrifuged by a high-speed

refrigerated centrifuge at 2,500 rpm for 5 minutes. The supernatant was collected and measured by a Shimadzu UV2550 ultraviolet-visible spectrophotometer (Japan) at 545 nm. ODs of the six MIL tubes, tube 7, and tube 8 were referred to as ODt, ODnc and ODpc, respectively. The hemolysis rate was calculated as from the formula hemolysis rate (%) = (ODt – ODnc)/(ODpc – ODnc) ×100%, and the experiment was repeated three times.

The platelet-aggregation rate was also measured to determine MIL's effect on platelets. In brief, blood collected from fasting New Zealand rabbits was mixed with sodium citrate (109 mM) at a ratio of 9:1 and centrifuged at 555 *g* for 10 minutes at room temperature to make platelet-rich plasma. This was diluted to 300×10^9 cells per liter, and poured into seven tubes; the first tube was filled with 50 µL of saline as a negative control, whereas the next six tubes were filled with 50 µL purified MIL containing rhIFNα_2b at the following concentrations: 2,000, 4,000, 6,000, 8,000, 10,000, or 12,000 IU/mL. All tubes were then incubated in a water bath at 37°C for 15 minutes. Platelet-aggregation rates were calculated using a Chrono-Log aggregometer (USA).

Nitroblue tetrazolium (NBT)-reducing testing was further performed to determine MIL's effect on the change in leukocyte absolute numbers and its relative phagocytic activity. Sprague Dawley rats (weight 180–200 g) were divided into seven groups (n=10), with equal numbers of males and females in each group. Each group was intravenously injected with either saline (NS) or MIL with the following concentrations of rhIFNα_2b (2,000, 4,000, 6,000, 8,000, 10,000, or 12,000 IU/mL). Blood was collected 1 hour following injection and mixed with an equal volume of 2% NBT solution. Samples were incubated at 37°C for 15 minutes before fixed with methanol. Giemsa–Wright dye was used to stain NBT-positive leukocytes, which were observed under a microscope to assess the absolute numbers and the phagocytic activity of leukocytes.

Acute-toxicity test

For the acute-toxicity test, 40 clean ICR mice (6–8 weeks old, 18–22 g) were randomly divided into four groups (n=10), with equal numbers of male and female mice in each group. Mice in the same group were intravenously injected with either purified MIL containing rhIFNα_2b at 2×10^6 IU, 1×10^6 IU, or 0.5×10^6 IU, or saline. The animals were kept at room temperature with about 60% humidity and natural light for 12 hours each day, fed with standard solid composite feedstuff, and received tap water ad libitum. All mice were routinely observed for around 1 week to record their spontaneous activity, muscular movements, muscle tension, reaction, autonomic nerve movement, breathing, skin color, and death. Mice were also weighed on the third and eighth day after injection, and then killed by cervical dislocation. Hearts, livers, spleens, lungs, kidneys, stomachs, intestines, and the thymus were collected for further pathologic anatomical examination.

Cell-apoptosis assays

Bel-7402 cells were divided into five groups, and each group was treated with the following doses of rhIFNα_2b: NS group, 0 IU/mL rhIFNα_2b; ML group, 0 IU/mL; IFN group, 10,000 IU/mL; IL group, 10,000 IU/mL; and MIL group, 10,000 IU/mL. An external magnetic field with a strength of 5,000 G was applied to the bottom of a 96-well plate for 30 minutes, and the plate was incubated at 37°C for 24 hours. Cells were washed with PBS three times and fixed in 3.7% paraformaldehyde in PBS for 15 minutes at room temperature. Cells were covered with methanol for 15 minutes at room temperature, and then washed with PBS. Afterward, cells were incubated with acridine orange staining solution and then observed with a laser scanning confocal microscope (LaVision BioTec, Germany) at 488 nm excitation, and 515 nm-emission wavelengths.

Caspase-3 activity in cells was also analyzed using a caspase-3 colorimetric assay kit (BioVision, USA) to detect apoptosis induction. As described earlier, cells were treated with NS, IFN, IL, ML, or MIL. An external magnetic field of 5,000 G was applied to the cells for 30 minutes, and cells were further incubated at 37°C for 24 hours. Cells were then lysed at 4°C for 10 minutes, and centrifuged at 10,000 *g* for 1 minute. The same amount of total protein was incubated in a 96-well plate with 0.2 mM acetyl-Asp-Glu-Val-Asp *p*-nitroanilide (Ac-DEVD-pNA) at 37°C for 1 hour. OD at 405 nm was measured using the colorimetric assay kit, and concentrations of pNA were calculated.

MTT cell-proliferation assay

Bel-7402 cells at the logarithmic phase (100 µL/well [2×10^4 cells]) were plated and cultured in a 96-well plate at 37°C. Twenty-four hours later, 100 µL of RPMI 1,640 medium without phenol red (0.4% fetal bovine serum) was added to each well to replace the culture medium. Cells were then incubated further at 37°C for 24 hours. All wells in the plate were then divided and incubated with the following media: RPMI 1640 medium, NS group; ML, ML group; free rhIFNα_2b, IFN group; IL, IL group; and MIL, MIL group. Later, wells containing the IFN, IL, and MIL groups were

further divided into six subgroups and incubated with different concentrations of rhIFNα_2b (15,000, 12,000, 10,000, 1,000, 100, and 50 IU/mL). Triplicates were set up for each treatment, and three wells were used to determine statistical difference. After addition of the drugs, a magnetic field ($Nd_2Fe_{12}B$ magnet tablets) with a strength of 5,000 G was applied to the bottom of the plate for 30 minutes. The cells were further cultured at 37°C, 95% relative humidity, and 5% CO_2 for 48 hours. Afterward, 10 μL of MTT reagent was added to each well, and the plate was again incubated at 37°C for 4 hours. Finally, 100 μL of detergent reagent was added to each well to replace the media, and cells were stored at room temperature in the dark for 2 hours. ODs at 570 nm were measured to determine the reduction of MTT. The cell growth-inhibition ratio was calculated as ([1– OD-treated group]/OD control group) ×100%.

Pharmacokinetic and tissue-distribution studies

A total of 120 ICR mice (weight 18–22 g) were randomly divided into three groups, with equal numbers of male and female mice in each group. Mice in the same group were either intravenously injected with 10 ng/g body weight of free rhIFNα_2b (group A) or MIL (groups B and C). Mice in group C were then given $Nd_2Fe_{12}B$ permanent magnet tablets (Halde GAC, Spain) on the surface of the skin where the kidney was located to produce a magnetic field strength of 5,000 G. Each group of mice was randomly divided further into eight subgroups, with five mice in each group. Blood was collected from the mice in each subgroup by enucleating mice eyeballs at eight different time points (10, 30, 60, 120, 180, 240, 300, and 480 minutes). All blood samples were centrifuged for 10 minutes at 8,000 rpm to collect plasma, and all of the samples were stored at −20°C. The plasma rhIFNα_2b concentrations were determined by ELISA assay, and pharmacokinetic parameters were determined by 3p97 software.

For the tissue-distribution study, mice were killed as previously described to obtain hearts, livers, spleens, lungs, and kidneys after blood collection. After the removal of fatty and connective tissue, the remaining tissues were washed with saline and dried on filter paper. Around 0.5–1.0 g of each tissue sample was cut into pieces and treated with 1 mL of saline. Samples were subsequently homogenized and centrifuged at 8,000 rpm for 10 minutes. The supernatant was collected and diluted with saline. Finally, the concentration of rhIFNα_2b in each tissue sample at different time points was determined by ELISA and plotted to yield a curve.

Targeting MIL on mice hepatocellular carcinoma

BALB/c nude mice were xenografted with HCC tumors by inoculating Bel-7402 cells in their livers. When the tumors ranged from 6 mm to 8 mm in diameter, 30 tumor-bearing nude mice were randomly and equally divided into five groups and given one of the following treatments: saline, free rhIFNα_2b, IL, ML, or MIL. Around 200 μL of each treatment was injected through the caudal vein of each mouse. $Nd_2Fe_{12}B$ magnet tablets were fastened to the skins surrounding the tumor areas in the ML and MIL groups of mice, and magnetic fields (5,000 G) were applied to the tumor surfaces for 30 minutes. Treatments were repeated three times over an interval of 3 days. Two perpendicular diameters of tumors were measured at intervals of 6 days using a slide caliper. Tumor volumes were calculated using the formula 0.5 ($a \times b^2$), where a and b were the longest and shortest dimensions (mm) of the tumor, respectively. On day 30, the mice were killed as previously described in the "Acute-toxicity test" section, and their tumors were collected, weighed, and compared. The tumor-inhibition rate based on the tumor-weight change was calculated according to the following equation:

$$\text{Tumor-inhibition rate} = ([Mc - Me]/Mc) \times 100\%, \quad (3)$$

here, *Mc* refers to the average tumor weight of the saline group and *Me* refers to the average tumor weight of all the other groups.

Real-time quantitative RT-PCR

Mice were killed by cervical dislocation on day 30, and liver tumors were collected. Total ribonucleic acid (RNA) from tumor tissues was isolated using Trizol reagent. Real-time quantitative reverse-transcription polymerase chain reactions (RT-PCRs) were performed using an iScript one-step RT-PCR kit with SYBR green dyes (Bio-Rad). The sequences of primers were designed as follows: for Bcl-2, the forward primer was 5′-TTGGATCAGGGAGTTGGAAG-3′, and the reverse was 5′-TGTCCCTACCAACCAGAAGG-3′; for Bax, the forward primer was 5′-AGGATGCGTCCACCAAGAAG-3′, and the reverse was 5′-GAGTCTCACCCAACCACCCT-3′; and for glyceraldehyde 3-phosphate dehydrogenase (GAPDH), the forward primer was 5′-GCCAAAAGGGTCATCATCTC-3′, and the reverse was 5′-GCCTTCAACGCCTGCTTC-3′. Thirty PCR cycles were utilized, and each cycle consisted of 95°C for 30 seconds, 55°C for 30 seconds, and 68°C for 60 seconds, with an initial denaturation step of 95°C for 5 minutes and a final elongation step of 68°C for 10 minutes. The RNA amount was standardized by quantitation of GADPH

messenger RNA (mRNA), and all values were expressed relative to GADPH. Statistical analysis was performed on three independent replicates for each RNA sample.

Western blots

Tumor samples were homogenized for protein isolation. Briefly, frozen tissues were cut into small pieces of about 2 mm in diameter on ice, placed into a tube containing solution A (10 mM Tris acetate, 6 mM 2-mercaptoethanol, 1 mM ethylene glycol tetraacetic acid, 4 mM $MgCl_2$, 0.5% Triton X-100, 1 mM phenylmethanesulfonyl fluoride, 1 mM tosyl phenylalanyl chloromethyl ketone, leupeptin, pepstatin, aprotinin, and sodium azide), vortexed, homogenized, and centrifuged. The supernatant was collected, and protein concentrations were determined by BCA protein assays (Pierce). Around 50 μg of each protein sample was run on 10% sodium dodecyl sulfate polyacrylamide gel electrophoresis and further transferred onto a polyvinylidene difluoride membrane at 150 V for 1 hour. The membrane was blocked with 5% nonfat dry milk in 1% Triton X-100 containing Tris-buffered saline (TBS) buffer at 4°C overnight and probed with a rabbit antihuman Bcl-2 (or Bax) polyclonal antibody as the primary antibody at 1:500 ratio under room temperature for 2 hours. After washing with TBS + 0. 1% Tween buffer four times, the membranes were incubated with horseradish peroxidase-conjugated goat antirabbit IgG as the secondary antibody at a ratio of 1:2,000 at room temperature for 1.5 hours. The membranes were further washed with TBS + Tween buffer and developed on X-ray film using an enhanced chemiluminescence buffer. The films were scanned and quantitated using NIH Image version 1.61 (National Institutes of Health, US), and the quantities of Bcl-2 (or Bax) protein were standardized against β-actin as an internal control.

Statistical analysis

One-way analysis of variance and two sample *t*-tests were used to determine significant differences between groups. Statistical significance was established at $P<0.05$. Analyses were performed using the standard statistical software SPSS 20.0.

Results

Preparation and characterization of MIL

To improve rhIFNα_2b transport and enhance its therapeutic effects against HCC, we employed ML as a carrier and developed a novel MIL that successfully encapsulated the drug. MIL was synthesized using a combined method of reverse-phase evaporation and ice-water bath ultrasonication. This novel method dramatically improved MIL stabilization and drug-encapsulation efficiency. The developed MIL can be further purified from free rhIFNα_2b and ML particles using Sephadex G-50 beads (Figure S1).

We tested for the development of MIL with three lipid compositions. When the molar ratio of PC/Chol/DMPG was 6:4:1, the mean diameter of MIL obtained by DLS was about 170 nm, which was not significantly different from that obtained at a PC/Chol/DMPG molar ratio of 6:3:0 (≈152 nm) (Figure 1A). However, when the molar ratio of Chol was further enhanced (6:5:1), the mean diameter of the resultant MIL particles dramatically increased to 253 nm (Figure 1A), which indicates that Chol enlarged the size of the MIL particles, perhaps because of its bulk size. The PI was also measured by DLS to determine the size distributions of MIL in all three different lipid mixtures. As shown in Figure 1B, the smallest index among the three samples was close to 0.3, which indicates that this lipid composition produced the most homogeneous particle sizes. The PIs of the two other lipid compositions were both over two times larger than 0.3.

We then determined the drug-encapsulation efficiency of all developed MIL by ELISA using antihuman rhIFNα_2b antibody. As shown in Figure 1C, the drug-encapsulation efficiency of MIL with a PC/Chol/DMPG molar ratio of 6:4:1 was around 63%, which was slightly higher than those of the two other MILs (47% and 57% for ratios of 6:3:0 and 6:5:1, respectively). Moreover, when the molar ratio was at 6:4:1, the MIL yield was also slightly higher than those obtained at the two other ratios (Figure 1D). All of the data confirm that the MIL developed using a PC/Chol/DMPG molar ratio of 6:4:1 shows excellent characteristics. Unless otherwise specified, subsequent assays in this work employed MILs with a PC/Chol/DMPG molar ratio of 6:4:1.

We observed the morphology of the developed MIL by transmission electron microscopy. As shown in Figure 1E, the Fe_3O_4 NPs only had a mean diameter of 10 nm. In contrast, MIL particles were around 170 nm in mean diameter, as confirmed by DLS, and were significantly larger than Fe_3O_4 NPs (Figures 1F and S2). MIL particles were close to spherical in shape, and the surfaces of the particles were smooth. To determine whether the novel MIL encapsulated MNPs and maintained their magnetic property, we compared the appearance of MIL suspensions with and without a strong $Nd_2Fe_{12}B$ magnet placed next to the ampoule. With a strong magnetic field, the MIL suspension exhibited a positive reaction, and nearly all of the MIL moved toward one side of the ampoule within 30 seconds (Figure S3A). However,

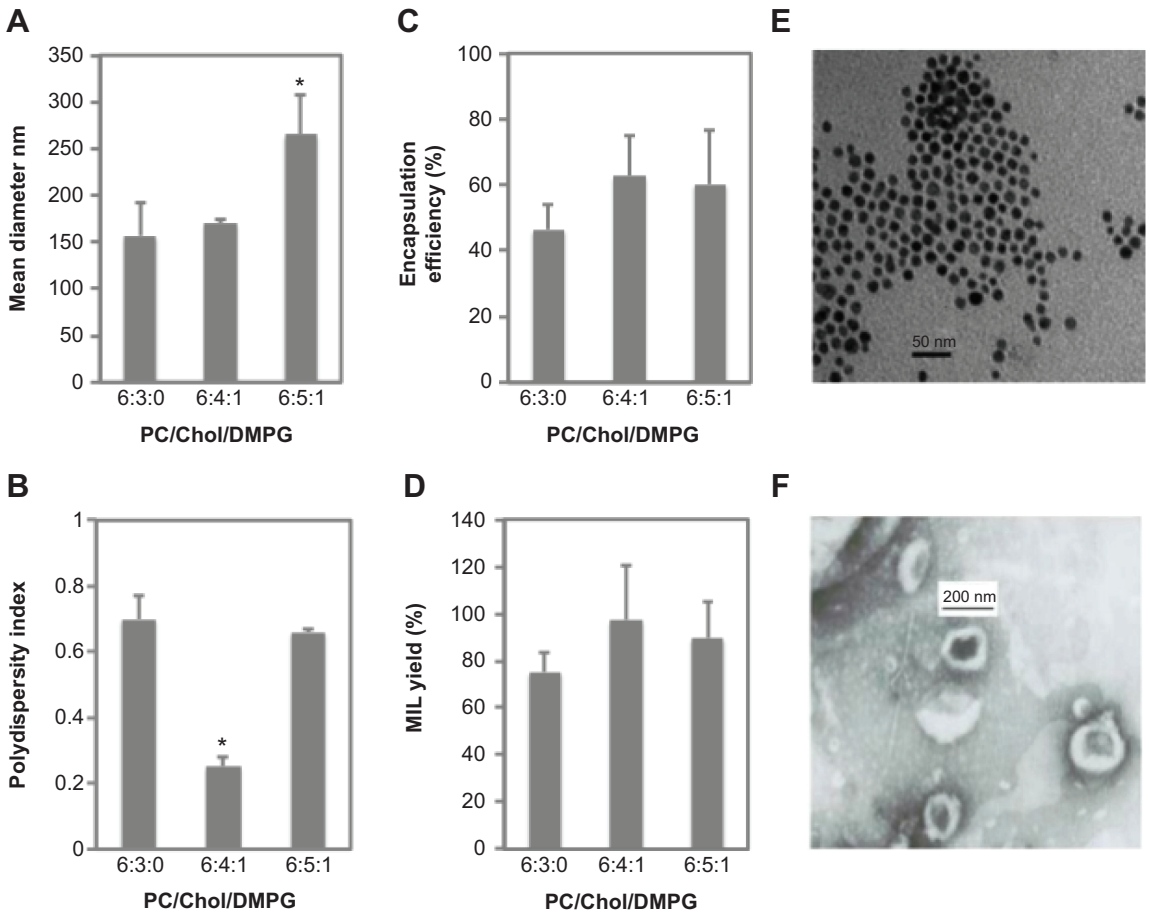

Figure 1 Preparation and characterization of magnetoliposomes containing recombinant human IFNα$_2$b (MIL).
Notes: (**A**) Mean diameters of MIL were determined using dynamic light scattering with different molar ratios of the following lipids: phosphatidylcholine (PC), cholesterol (Chol), and 1,2-dimyristoyl-*sn*-glycero-3-phosphoglycerol (DMPG), in Tris buffer at 25°C. (**B**) Plot of polydispersity indexes of MIL under different molar ratios of PC/Chol/DMPG. (**C**) Plot of drug-encapsulation efficiency of MIL under different molar ratios of PC/Chol/DMPG. (**D**) Plot of MIL yields with different molar ratios of PC/Chol/DMPG. (**E**) Transmission electron microscopy image of Fe_3O_4. Bar =50 nm; the mean diameter of Fe_3O_4 was 10 nm. (**F**) Transmission electron microscopy image of MIL. Bar =200 nm; the mean diameter of MIL was 170 nm. *Significant difference when compared with lipid composition 6:3:0 ($P<0.05$).

without a magnet field, the MIL solution was homogeneous and appeared brownish in color (Figure S3B).

We further characterized the effects of temperature and duration of storage on MIL stability by comparing the mean size and drug encapsulation efficiency before and after 6 months of storage at 4°C or –20°C. As expected, no significant differences were found between each MIL group, which suggests that the particles were stable enough for further studies (Figure S4). Irradiation sterilization did not affect the particle size or drug-entrapment efficiency of the developed MIL either (Figure S5).

Biological safety of MIL for cells and animals

To determine whether our novel MIL was suitable for clinical studies, we evaluated its biological safety to rabbit blood cells by performing in vitro hemolytic tests. Three different types of blood cells – erythrocytes, platelets, and leukocytes – were tested. First, erythrocytes were incubated in eight test tubes with MIL, saline (no hemolysis), or distilled water (complete hemolysis). Four different outcomes, including complete hemolysis, partial hemolysis, no hemolysis, and cohesion, were expected in this test. As shown in Table 1, all of the hemolysis rates in tubes with MIL were lower than

Table 1 Magnetoliposomes containing recombinant human IFNα$_2$b hemolysis test results (spectrophotometry) (n=5)

Group	ODt – ODnc	ODpc – ODnc	Hemolysis rate (%)	Macroscopic observation
1	0.0148	0.425	3.48	–
2	0.0150	0.425	3.53	–
3	0.0164	0.425	3.86	–
4	0.0171	0.425	4.02	–
5	0.0183	0.425	4.31	–
6	0.0179	0.425	4.21	–

Note: –, no hemolysis.

5%, which indicates that no significant hemolysis occurred in these tubes.

Next, we evaluated the effect of MIL on the function of platelets by measuring the platelet-aggregation rate using the Chrono-Log aggregometer. As shown in Figure S6A, significantly different platelet-aggregation rates were neither observed between the control and MIL groups, nor among MIL groups, which indicates that MIL had no devastating effects on platelets. Finally, the effects of MIL on leukocyte absolute numbers and phagocytic activity were also examined. The absolute numbers of three different leukocytes – white blood cells, polymorphonuclear leukocytes, and lymphocytes – were individually examined. Our results showed that no significant differences on leukocytes absolute numbers were observed between the control and MIL groups, nor among MIL groups, in all three different leukocytes (Figure S6, B–D). Phagocytic activities of leukocytes were all similar between the control and MIL groups, and among MIL groups (Figure S6E). Therefore, we conclude that MIL does not affect blood-cell integrity, which suggests that it is safe to use for rhIFNα_2b delivery.

We then examined the biological safety of MIL for the whole animal by performing acute-toxicity tests. In brief, ICR mice were treated with either MIL containing various concentrations of rhIFNα_2b or saline. No unusual behavior or appearance (such as making abnormal sounds, tremors, convulsion, ataxia, salivation, lacrimation, runny nose, breathing problems, constipation, bowel bilging gas, urinary incontinence, depilation, decrustation, erosion of the skin, inflammation, redness, or swelling) (Table S1) was observed in any group of mice. In fact, some active behaviors, such as ear scratching, licking of the feet, and moving of the head, were observed in MIL groups. All of the MIL groups also showed good appetites, normal excrement grain, shiny fur, and fleshy red claws and tails compared with the saline group (Table S1). None of the mice died after MIL injection. Mice injected with different dosages of MIL behaved normally, similar to the saline group, which indicates that MIL presents no acute toxicity to mice.

During this study, the mice body weights were also recorded at the third and eighth days after MIL injection. As expected, all of the mice showed slightly increased body weights at both time points, which further confirms that MIL exerts no acute toxicity toward mice (Table S2). No significant difference was found between the body weights of each group on the same day. Mice were killed by cervical dislocation and dissected on day 8, and all organs, including the heart, liver, spleen, lungs, kidneys, stomach, intestines, and thymus, were pathologically examined. Again, no significant changes in the organs were detected (data not shown). Overall, our data suggest that MIL does not induce acute toxicity when delivered to the animal.

Pharmacokinetic and tissue-distribution studies

Whether MIL delivered into animals maintains its magnetic behavior is not clear. How long MIL is accumulated at the target location is also unknown. Therefore, we examined the pharmacokinetics of MIL in mice. Here, three groups of mice (A, free rhIFNα_2b group; B, MIL group; and C, MIL + magnet group) were utilized, and plasma concentrations of rhIFNα_2b were determined by ELISA assay at various time points. As shown in Figure 2A, levels of plasma rhIFNα_2b in all groups increased after injection and reached maximum amounts after 30 minutes. Plasma rhIFNα_2b levels in all groups continuously declined thereafter with time. Except at 500 minutes following injection, plasma rhIFNα_2b levels in group C were significantly lower than those in groups A and B, which suggests that the novel particles deliver rhIFNα_2b to target tissues rather than being suspended in blood vessels (Figure 2A).

To confirm our hypothesis, we examined the rhIFNα_2b concentrations in a variety of mouse tissues, including the spleen, liver, kidneys, lungs, and heart, by ELISA. Data obtained were fitted as curves according to specific time points (Figure 2B–F). In contrast to levels of plasma rhIFNα_2b, at each time point, levels of rhIFNα_2b in every tissue from group C were higher than those in tissues of groups A and B, which confirms that the magnet tablet indeed helps distribute MIL to the different tissues. As expected, the highest concentrations of rhIFNα_2b were observed in kidney tissues from group C 30 minutes after MIL injection (Figure 2D). Consistent with plasma rhIFNα_2b levels, the highest levels of rhIFNα_2b in all tissues were also detected 30 minutes after injection. Continuous declines were observed with further extensions of time in all tissues, except in the liver and kidney from group C (Figure 2C and D). The data suggest that an external magnetic field not only helps accumulate MIL in target locations (eg, the kidney) but also helps remove MIL from blood vessels. Only the curves for kidneys and livers from group C showed two peaks at 30 and 180 minutes, respectively, although details of this phenomenon are unknown. This second distribution peak was not found in other tissues from group C.

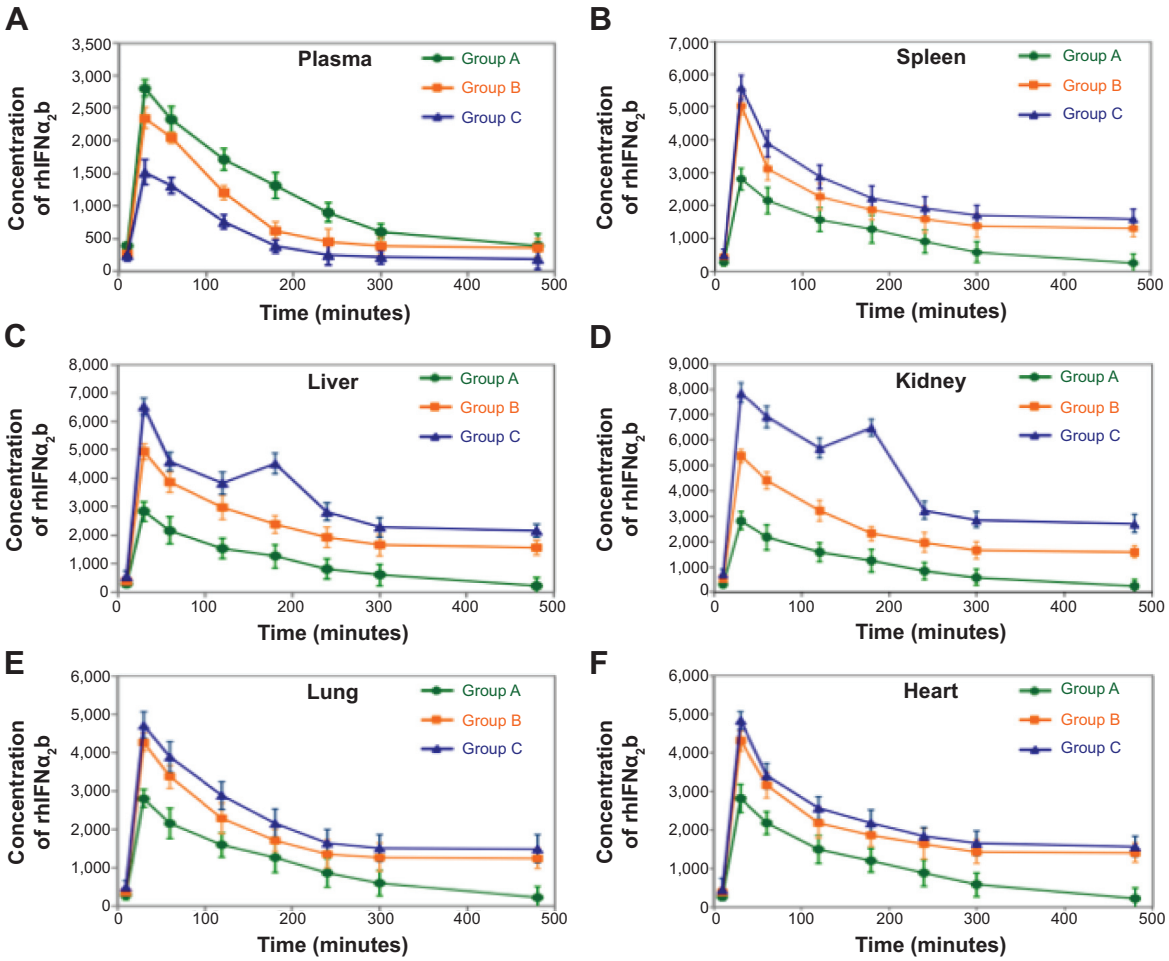

Figure 2 Pharmacokinetic and tissue-distribution studies of magnetoliposomes containing recombinant human (rh)-IFNα$_2$b (MIL) in animals.
Notes: (**A**) Plot of plasma rhIFNα$_2$b concentrations at eight different time points (10, 30, 60, 120, 180, 240, 300, and 480 minutes) from three groups of mice intravenously injected with free rhIFNα$_2$b (group A), and MIL (groups B and C). Group C mice were given external magnetic tablets, whereas group B mice were not. (**B**) Plot of rhIFNα$_2$b concentrations in spleen tissues. (**C**) Plot of rhIFNα$_2$b concentrations in liver tissues. (**D**) Plot of rhIFNα$_2$b concentrations in kidney tissues. (**E**) Plot of rhIFNα$_2$b concentrations in lung tissues. (**F**) Plot of rhIFNα$_2$b concentrations in heart tissues.

MIL inhibits cell growth

Encapsulation into ML does not affect the magnetic properties of the MNPs at all. However, whether this process affects the therapeutic effect of the drug is not yet clear. We tested the therapeutic effect of MIL on cells of the living hepatoma cell line Bel-7402. Five groups of cells incubated with NS, ML, IFN, IL, and MIL were set up, and cell viabilities were determined by MTT assay. As shown in Figure 3A, compared with the NS group, the IFN, IL, and MIL groups showed inhibition of Bel-7402 cell growth in a dose-dependent manner, whereas ML treatment showed little effect on cell growth. The inhibitory rates of the IL and MIL groups were both significantly higher than that of the IFN group, and no significant difference was observed between inhibitory rates in the IL and MIL groups. These data suggest that encapsulation of rhIFNα$_2$b with hydrophobic liposome particles can help transport rhIFNα$_2$b into living cells. The results also indicate that only the drug, and not the MNPs, inhibits cell growth. More importantly, the data confirm that the drug encapsulated in ML allows more extensive inhibition of tumor-cell growth than the free drug.

Next, we performed cell-imaging studies by laser scanning confocal microscope to further confirm whether the drug maintains its activity after encapsulation into ML. Here, cells in the same groups as earlier were stained with acridine orange to detect cell apoptosis. In the absence of drug treatment (NS and ML groups), cells showed uniform green fluorescence distributed all over the cell body (Figure 3B). However, during drug-induced cell apoptosis, clear morphological changes, such as chromatic agglutination, karyopyknosis, and nuclear fragmentation, could be observed even in cells with intact integral structures and morphology. As shown in Figure 3B, our results confirm that the IL and MIL groups exhibited the strongest drug effects in living cells.

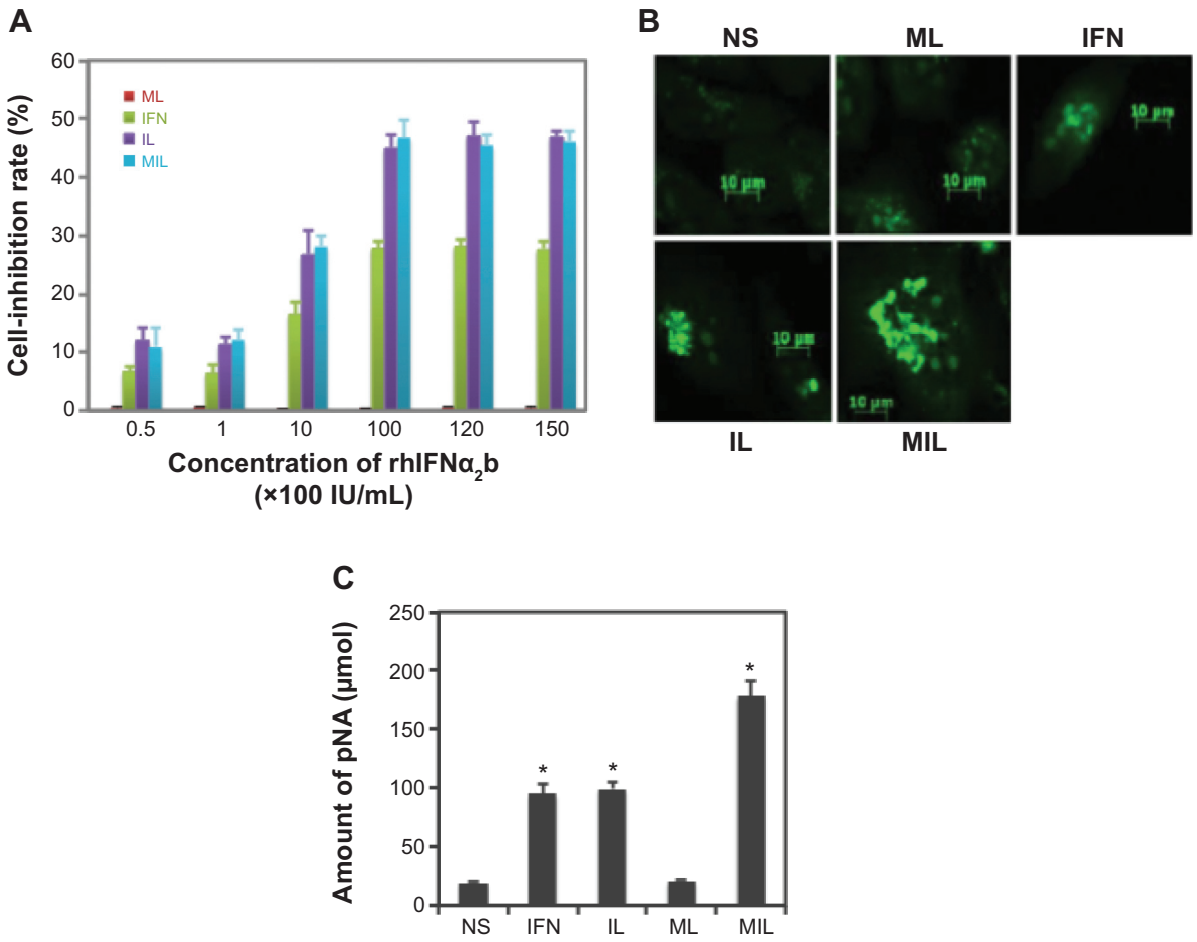

Figure 3 Magnetoliposomes (MLs) containing recombinant human (rh)-IFNα$_2$b (MIL) inhibit the growth of hepatoma cancer Bel-7402 cells.
Notes: (**A**) Inhibitory rates of Bel-7402 cells in the experimental (ML, IFNα$_2$b [IFN], IFNα$_2$b liposome [IL], and MIL) groups and control (NS) group. (**B**) Acridine orange test results of Bel-7402 cells treated with NS, IFN, IL, ML, and MIL for 24 hours. (**C**) Concentrations of *p*-nitroanilide (pNA) from five different groups treated with NS, IFN, IL, ML, and MIL were determined by measuring optical density values at 405 nm with colorimetric kits. *Significant difference when compared with the NS group ($P<0.05$).

When cells are in apoptosis, a sensitive protease caspase-3 is activated, and can be detected using a colorimetric kit by measuring the production of pNA from substrate Ac-DEVD-pNA. We incubated cells with five following solutions: NS, IFN, IL, ML, or MIL. The amount of pNA in each group was determined using a colorimetric kit. As shown in Figure 3C, the pNA amount in MIL group was the highest in all groups, around ten times that of the NS group, whereas the amounts of pNA in groups IFN and IL were around five times that of the NS group. No significant differences were observed between the NS and ML groups. These data further confirm that the drug, not the MNPs, inhibited cell growth, and that MIL had the biggest effect on cell-growth inhibition.

MIL inhibits the growth of liver tumors

Although the therapeutic activity of MIL in inhibiting tumor-cell growth has previously been proven, its efficiency in inhibiting tumor growth and reducing tumor size in animals is as yet unknown. Here, mice bearing HCC were separated into five different groups, and treated with either NS, ML, IFN, IL, or MIL. Tumor sizes were recorded at six different time points after injection with intervals of 6 days between each of them. As shown in Figure 4A, tumor size significantly decreased in MIL-treated mice compared with the control mice (NS group). Tumor size showed only slight changes in the IL and IFN groups, and no change in the ML group.

During this study, tumor sizes were calculated at intervals of 6 days (Figure 4, B and C). Again, tumor sizes were significantly reduced in all groups except the control group. The largest reductions were observed in the MIL group. The mean weight of tumors in the MIL group was around 565 mg, which was significantly lower than those obtained in other groups (eg, the IFN group showed a mean tumor weight of 1,091 mg, while the IL group showed a mean tumor weight

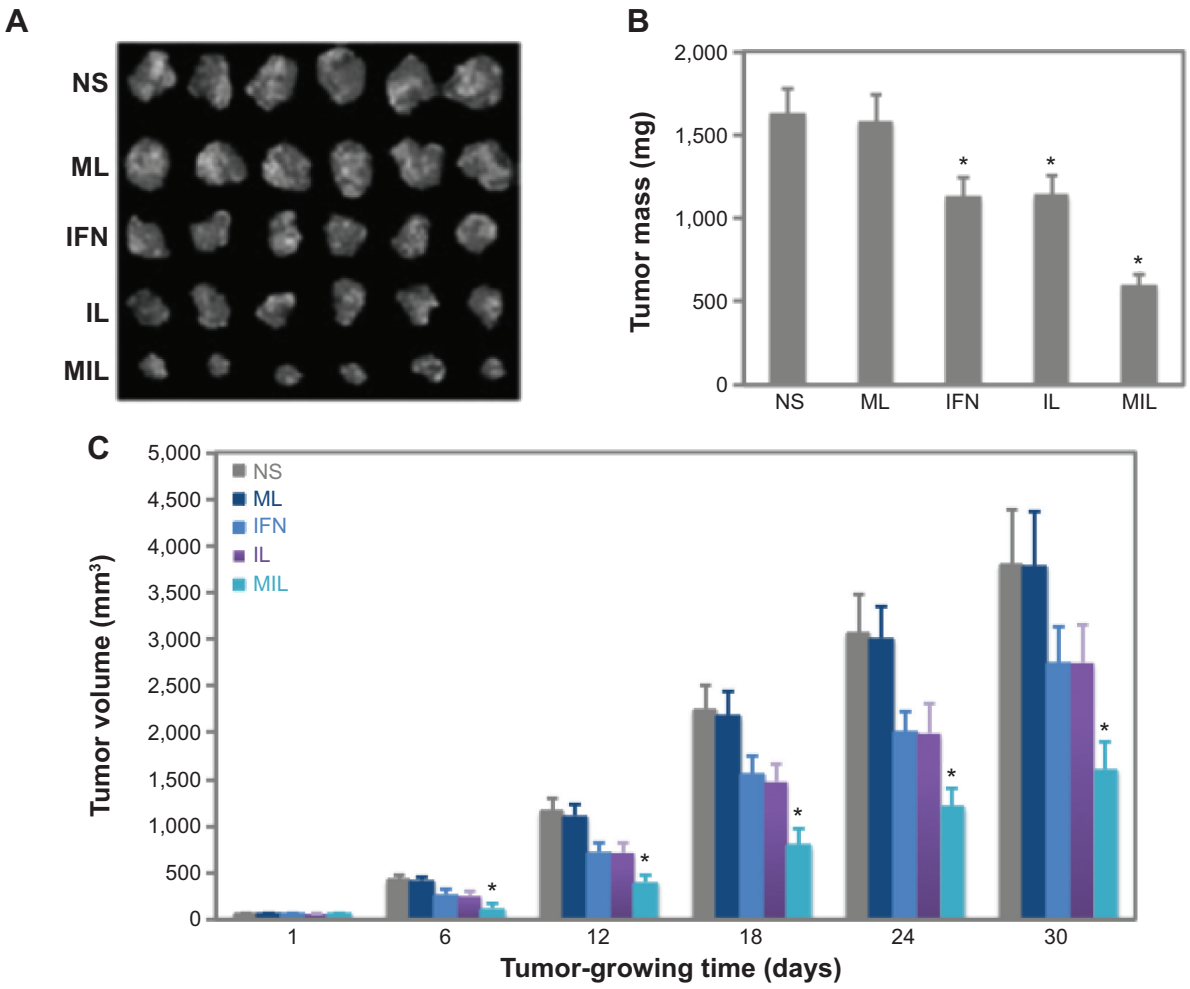

Figure 4 Magnetoliposomes (MLs) containing recombinant human (rh)-IFNα2b (MIL) inhibit liver tumor growth.
Notes: (**A**) Tumors collected from nude mice in different groups (n=6). (**B**) Plot of tumor masses from nude mice in different groups. (**C**) Comparison of tumor volumes of nude mice among different groups (n=6): saline NS, containing 0 IU rh-IFNα2b; ML, containing 0 IU rh-IFNα2b; IFN, containing 10,000 IU rh-IFNα2b; IL, containing 1,000 IU rh-IFNα2b; and MIL, containing 1,000 IU rh-IFNα2b. *Significant difference when compared with the NS group ($P<0.05$).

of 1,083 mg). MIL treatment efficiently inhibited tumor growth and reduced tumor sizes to 38% of the tumors in the NS group. Only slight reductions in tumor size (28%) were observed in the IFN and IL groups. ML treatment showed no effect on tumor inhibition: the mean weight of tumors in this group of mice was about 1,485 mg, which was nearly equal to the mean tumor weight of mice in the control group (1,508 mg, Figure 4B). Overall, our data suggest that targeted therapy with MIL could efficiently improve drug effects for treating HCC (Figure 4).

MIL activates cell apoptosis in liver tumors

MIL has been suggested to inhibit cell growth by activating cell apoptosis, as evidenced by our in vitro cell growth-inhibition study. However, whether MIL also induces cell apoptosis in living animals is not clear. Therefore, we examined the transcription and expression levels of two proteins, Bax and Bcl-2, which are well known as cell-apoptosis markers.

First, we examined the transcription levels of Bcl-2 and Bax in all of the collected tumor tissues. The RNA amount measured by quantitative real-time RT-PCR was standardized by quantitation of GADPH mRNA. As shown in Figure 5A, mRNA levels of Bax in the MIL group were the highest among all of the groups tested (right panel). Levels of Bax mRNA in the IFN and IL groups were also significantly higher than those in the NS and ML groups, and no significant difference was detected between the NS and ML groups. By contrast, mRNA levels of Bcl-2 were lowest in the MIL group, whereas mRNA levels of Bcl-2 in the IFN and IL groups were also significantly lower than those in the NS and ML groups (Figure 5A, left panel).

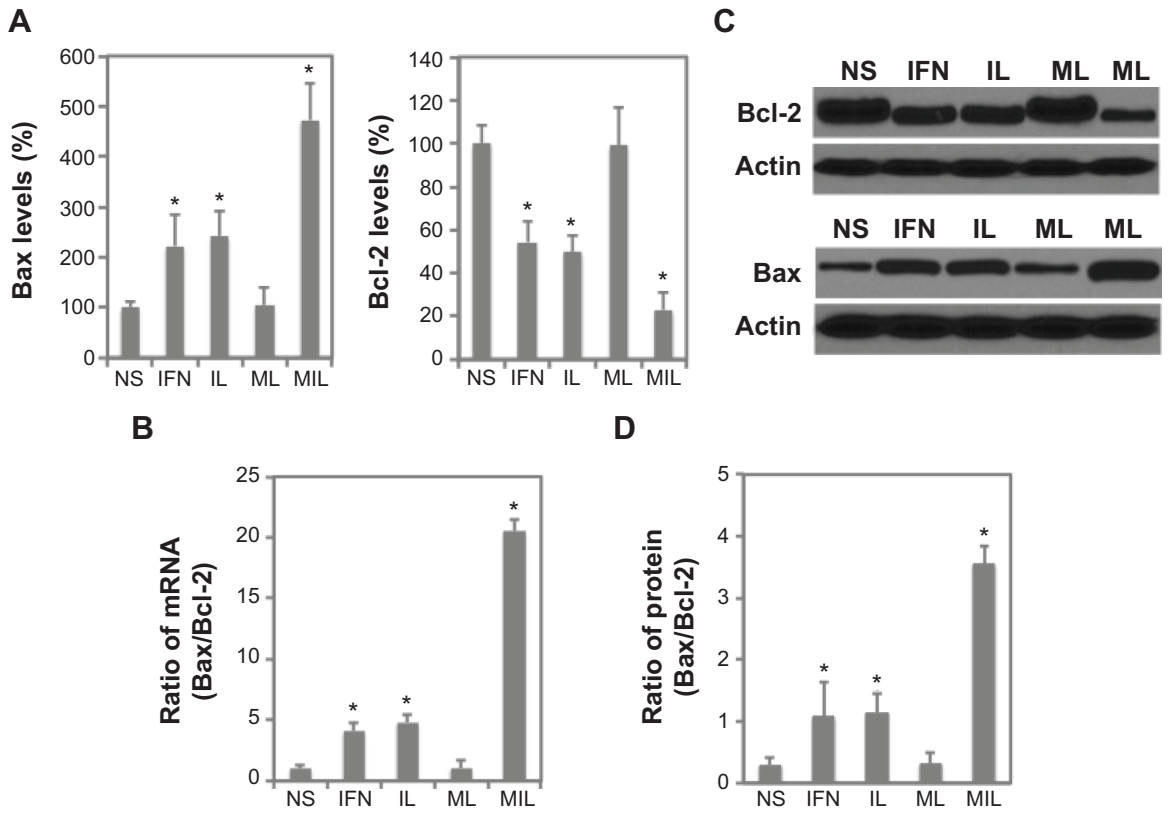

Figure 5 Magnetoliposomes (MLs) containing recombinant human IFNα_2b (MIL) activate cell apoptosis in liver tumors.
Notes: (**A**) Quantitative real-time reverse-transcription polymerase chain-reaction results show the transcription levels of Bax and Bcl-2 in tumor samples obtained from mice of five different groups (saline [NS], IFNα_2b [IFN], IFNα_2b liposome [IL], ML, and MIL groups). The right panel shows the relative messenger ribonucleic acid (mRNA) levels of Bax in the five groups, whereas the left panel shows the relative mRNA levels of Bcl-2 in the five groups. (**B**) Ratio of Bax/Bcl-2-transcription levels calculated from results of (**A**) in each group. (**C**) Western blot analysis shows Bax- and Bcl-2-expression levels in tumor tissues obtained from nude mice in different groups (NS, IFN, IL, ML, and MIL). (**D**) Ratio of Bax/Bcl-2 protein levels in tumor tissues of nude mice among the different groups, as determined from results of (**C**). *Significant difference when compared with the NS group ($P<0.05$).

The ratio of Bax to Bcl-2, rather than their absolute concentrations, is predictive of HCC apoptosis. As shown in Figure 5B, the Bax/Bcl-2 ratio in the MIL group was approximately 20 times higher than that in the NS group. Both the IFN and IL groups showed fivefold-higher Bax/Bcl-2 ratios than the NS group, whereas the ML group showed no significant difference in Bax/Bcl-2 ratio when compared with the NS group (Figure 5B). Overall, these results indicate that apoptosis pathways were also activated in tumor cells. The MIL group showed the highest tumor cell-apoptosis effects because of the high targeting efficiency and transport ability and low mass and volume of MIL particles.

Next, we examined Bax and Bcl-2 expression levels in all tumor tissues. Western blot analysis showed that the Bax protein level in the MIL group was highest among all of the groups tested, which was consistent with the mRNA levels of the same group determined earlier (Figure 5C). Bax protein levels in the IFN and IL groups were also significantly higher than those of the NS and ML groups. No significant difference in Bax levels between the IFN and IL groups or between the NS and ML groups was observed.

Western blot analysis showed that the Bcl-2 protein level in the MIL group was lowest among all of the groups tested, which further confirms previous findings (Figure 5C and D). Bcl-2 protein levels in the IFN and IL groups were significantly lower than those in the control and ML groups. Again, no significant difference in Bcl-2 protein levels was observed between the IFN and IL groups or between the NS and ML groups (Figure 5D). The protein level of the Bax/Bcl-2 ratio in the MIL group was significantly higher (12 times) than that in the NS group, which was consistent with the mRNA level of the group. These protein levels further confirm the hypothesis that MIL dramatically reduces tumor size by activating cell apoptosis through upregulation of the expression of the Bax protein with simultaneous downregulation of the expression of the Bcl-2 protein (Figure 5D).

Discussion

Drug therapy is the alternative treatment method employed when surgical resection or liver transplantation is precluded for HCC treatment.[3] However, cytotoxic chemotherapy of HCC is limited by severe and sometimes life-threatening side effects to other tissues, because these therapies are not selective for the liver organ only. One strategy to improve tissue specificity is to encapsulate the drug into a drug-delivery system capable of directing therapeutic compounds to a target site.[25] Increases in drug concentration and drug-residence time in the target area will greatly decrease drug toxicity in nontarget organs and further improve the effectiveness of the drug.

rhIFNα$_2$b is a good anticancer cytokine, especially for solid tumors, such as HCC.[3,8] It shows no antigenicity when delivered to human subjects, indicating it will not be neutralized by immune serum or destroyed by nucleases.[26] It has been suggested that rhIFNα$_2$b plays important roles in antitumor and antiviral activity and regulation of the immune system.[3,8–16] The mechanism of the antitumor effect is not completely clear yet. However, studies have suggested it might inhibit tumor growth in vivo through tumor cell-growth inhibition, tumor-cell apoptosis, oncogene-expression restraint, immune-system regulation, and tumor-angiogenesis suppression.[27–30]

Several methods have been described to directly deliver therapeutic genes or macromolecules to tumor targets.[31–35] For example, Mejías et al developed uniform dimercaptosuccinic acid-coated monodisperse MNPs as a delivery system to target the cytokine IFNγ to tumors.[32] The system dramatically improved the efficiency of IFNγ delivery, increasing local dosage without augmenting the systemic concentration, as well as reducing toxicity and other side effects. However, the drug was conjugated with free ligand groups on the surface of dimercaptosuccinic acid particles, making it vulnerable to being digested by enzymes in the bloodstream. Magnetofection combining a nonviral gene-transfer technology has also been developed to deliver the cytokine gene IFNγ into tumors.[33] However, this system needs DNA recombination between the endogenous and IFNγ genes, and leads to a higher probability of gene mutations. A novel delivery system was also developed with a NPs-containing indinavir into bone marrow-derived macrophages.[34–35] The system achieved therapeutic efficacy, improved drug distribution to areas of active viral replication, and extended dosing intervals. However, a macrophage is an immune cell that has the ability to infiltrate and accumulate in a variety of lesion sites, such as wounds, atherosclerosis plaques, and deep cancerous tissues, indicating the method has low specificity. In addition, the therapeutic macromolecules encapsulated in NPs are also prone to being digested by enzymes in macrophages.

In the present study, we used ML as a magnetic nanometer-scale drug carrier to encapsulate rhIFNα$_2$b and prepared MIL by reverse-phase evaporation combined with ice-water bath ultrasonication. The method requires the encapsulation of rhIFNα$_2$b into NPs, preventing the digestion of rhIFNα$_2$b by enzymes in blood or macrophages. In our system, we encapsulated proteins rather than genes as therapeutic drugs, avoiding potential DNA mutation in the cell. Most importantly, we can apply a magnetic field outside our system to specifically deliver drugs to the target tumors to improve therapeutic efficacy and reduce side effects to other nontarget organs. Overall, we believe our delivery system is much better than all of other systems described herein.

We performed several experiments to optimize synthesis conditions by varying the amounts of chloroform, ferrofluid particles, rhIFNα$_2$b, PC, Chol, DMPG, buffer type and concentration, temperature, rotary speed in the rotary flash evaporator, and duration in the ice-water bath ultrasonicator. As shown in Figure 1, the size of MIL depends on its lipid composition. For example, Chol increases the mean diameters of ML particles and renders them more rigid.[36] The extent of entrapment of macromolecules in ML is also influenced by its lipid composition and concentration, the size of the vesicles, and the preparation technique. The presence of a negatively charged lipid, such as DMPG, is necessary to form stable associations between rhIFNα$_2$b and ML. Incorporation of rhIFNα$_2$b into ML is improved when Chol is included in the lipid bilayer, likely because of the rigid structure of the molecule. Therefore, our novel synthesis method in combination with an optimized lipid composition is expected to increase both the encapsulation efficiency of rhIFNα$_2$b into MIL and the stability of MIL.

We showed that the synthesized MIL maintains the fundamental characteristics of drugs used for intravenous injection. Cell experiments and animal studies demonstrated that MIL dramatically inhibits cell growth and significantly reduces the tumor sizes in nude mice under the guidance of a magnetic field (Figures 3 and 4). Cytotoxic drugs used to treat malignancies were also shown to trigger apoptotic pathways. Bcl-2, an apoptosis inhibitor, can block programmed cell death without affecting cellular proliferation. By contrast, Bax, an apoptosis promoter, is a member of the Bcl-2 family, which promotes apoptosis.[37,38] Therefore, the ratio of Bax to Bcl-2 can be used to determine the susceptibility of a cell to apoptosis.[39,40] In this study, we evaluated the correlation

of Bax and Bcl-2 mRNA and protein levels with HCC by targeting MIL therapy of nude mice with human HCC under the guidance of a magnetic field. RT-PCR results showed that the mRNA expression of Bcl-2 in the MIL group was the lowest among all of the groups studied and that the mRNA expression of Bax in the MIL group was the highest among all of the groups surveyed (Figure 5, A and B). Western blot analysis showed similar results based on protein and mRNA levels (Figure 5, C and D). All the results confirmed that tumor-growth inhibition in nude mice was caused by cell apoptosis activated via rhIFNα_2b specifically delivered to the tumor site.

In summary, this study demonstrates that MIL, an ML encapsulated with the anticancer drug rhIFNα_2b, may achieve anticancer effects in the clinical settings. Therefore, targeted therapy could be a novel approach for cancer treatment and warrants further studies.

Acknowledgments

This work was partly supported by grants from the China Scholarship Council (201208330266), the Natural Science Foundation of Zhejiang Province, PRC (Y4110029 and Y4090379), and the Natural Science Foundation of Wenzhou Science Technology Bureau, Zhejiang, PRC (Y20100018). We appreciate Dr Matthew Wheeler at the Scripps Institute for editing the manuscript.

Disclosure

The authors report no conflicts of interest in this work.

References

1. Venook AP, Papandreou C, Furuse J, de Guevara LL. The incidence and epidemiology of hepatocellular carcinoma: a global and regional perspective. *Oncologist*. 2010;15 Suppl 4:5–13.
2. Yang JD, Roberts LR. Epidemiology and management of hepatocellular carcinoma. *Infect Dis Clin North Am*. 2010;24:899–919.
3. Yuen MF, Hon C, Hui CK, Siu CW, Lai CL. Recombinant interferon alfa 2b therapy in a patient with metastatic hepatocellular carcinoma. *J Clin Gastroenterol*. 2002;35:272–275.
4. Chua CW, Choo SP. Targeted therapy in hepatocellular carcinoma. *Int J Hepatol*. 2011;2011:1–9.
5. Le Buanec H, Gougeon ML, Mathian A, et al. IFN-α and CD46 stimulation are associated with active lupus and skew natural T regulatory cell differentiation to type 1 regulatory T (Tr1) cells. *Proc Natl Acad Sci U S A*. 2011;108:18995–19000.
6. Yi T, Elson P, Mitsuhashi M, et al. Phosphatase inhibitor, sodium stibogluconate, in combination with interferon (IFN) alpha 2b: phase I trials to identify pharmacodynamic and clinical effects. *Oncotarget*. 2011;2:1155–1164.
7. Shinohara N, Abe T, Sazawa A, et al. Interferon-alpha-based immunotherapy in metastatic renal cell carcinoma patients with the primary tumor in situ. *Jpn J Clin Oncol*. 2012;42:113–119.
8. Singal AK, Freeman DH Jr, Anand BS. Meta-analysis: interferon improves outcomes following ablation or resection of hepatocellular carcinoma. *Aliment Pharmacol Ther*. 2010;32:851–858.
9. Breitenstein S, Dimitroulis D, Petrowsky H, et al. Systematic review and meta-analysis of interferon after curative treatment of hepatocellular carcinoma in patients with viral hepatitis. *Br J Surg*. 2009;96:975–981.
10. Wang BX, Rahbar R, Fish EN. Interferon: current status and future prospects in cancer therapy. *J Interferon Cytokine Res*. 2011;31:545–552.
11. Lesinski GB, Raig ET, Guenterberg K, et al. IFN-alpha and bortezomib overcome Bcl-2 and Mcl-1 overexpression in melanoma cells by stimulating the extrinsic pathway of apoptosis. *Cancer Res*. 2008;68:8351–8360.
12. Satthaporn S, Aloysius MM, Robins RA, et al. Ex vivo recovery and activation of dysfunctional, anergic, monocyte-derived dendritic cells from patients with operable breast cancer: critical role of IFN-alpha. *BMC Immunol*. 2008;9:32.
13. Xuan C, Steward KK, Timmerman JM, Morrison SL. Targeted delivery of interferon-alpha via fusion to anti-CD20 results in potent antitumor activity against B-cell lymphoma. *Blood*. 2010;115:2864–2871.
14. Bukowski R, Ernstoff MS, Gore ME, et al. Pegylated interferon alfa-2b treatment for patients with solid tumors: a phase I/II study. *J Clin Oncol*. 2002;20:3841–3849.
15. Wang YS, Youngster S, Grace M, Bausch J, Bordens R, Wyss DF. Structural and biological characterization of pegylated recombinant interferon alpha-2b and its therapeutic implications. *Adv Drug Deliv Rev*. 2002;54:547–570.
16. Galor A, Karp CL, Chhabra S, Barnes S, Alfonso EC. Topical interferon alpha 2b eye-drops for treatment of ocular surface squamous neoplasia: a dose comparison study. *Br J Ophthalmol*. 2010;94:551–554.
17. García-Jimeno S, Escribano E, Queralt J, Estelrich J. External magnetic field-induced selective biodistribution of magnetoliposomes in mice. *Nanoscale Res Lett*. 2012;7:452.
18. Singh R, Nalwa HS. Medical applications of nanoparticles in biological imaging, cell labeling, antimicrobial agents, and anticancer nanodrugs. *J Biomed Nanotechnol*. 2011;7:489–503.
19. Solomon M, D'Souza GG. Recent progress in the therapeutic applications of nanotechnology. *Curr Opin Pediatr*. 2011;23:215–220.
20. Jing H, Wang J, Yang P, Ke X, Xia G, Chen B. Magnetic Fe_3O_4 nanoparticles and chemotherapy agents interact synergistically to induce apoptosis in lymphoma cells. *Int J Nanomedicine*. 2010;5:999–1004.
21. Wang C, Zhang H, Chen B, Yin H, Wang W. Study of the enhanced anticancer efficacy of gambogic acid on Capan-1 pancreatic cancer cells when mediated via magnetic Fe_3O_4 nanoparticles. *Int J Nanomedicine*. 2011;6:1929–1935.
22. Kawaguchi E, Shimokawa K, Ishii F. Physicochemical properties of structured phosphatidylcholine in drug carrier lipid emulsions for drug delivery systems. *Colloids Surf B Biointerfaces*. 2008;62:130–135.
23. Wang J, Chen Y, Chen B, et al. Pharmacokinetic parameters and tissue distribution of magnetic Fe(3)O(4) nanoparticles in mice. *Int J Nanomedicine*. 2010;5:861–866.
24. Kim MJ, Jang DH, Lee YI, Jung HS, Lee HJ, Choa YH. Preparation, characterization, cytotoxicity and drug release behavior of liposome-enveloped paclitaxel/Fe_3O_4 nanoparticles. *J Nanosci Nanotechnol*. 2011;11:889–893.
25. Cinti C, Taranta M, Naldi I, Grimaldi S. Newly engineered magnetic erythrocytes for sustained and targeted delivery of anti-cancer therapeutic compounds. *PloS One*. 2011;6:17132.
26. Einat M, Resnitzky D, Kimchi A. Close link between reduction of c-myc expression by interferon, and G0/G1 arrest. *Nature*. 1985;313:597–600.
27. Yamamoto-Yamaguchi Y, Okabe-Kado J, Kasukabe T, Honma Y. Induction of apoptosis by combined treatment with differentiation-inducing agents and interferon-alpha in human lung cancer cell. *Anticancer Res*. 2003;23:2537–2547.
28. Xu D, Erickson S, Szeps M, et al. Interferon alpha down-regulates telomerase reverse transcriptase and telomerase activity in human malignant and nonmalignant hematopoietic cells. *Blood*. 2000;96:4313–4318.

29. Azzimonti B, Pagano M, Mondini M, et al. Altered patterns of the interferon inducible gene IFI16 expression in head and neck squamous cell carcinoma: immunohistochemical study including correlation with retinoblastoma protein, human papillomavirus infection and proliferation index. *Histopathology*. 2004;45:560–572.
30. Matsui W, Huff CA, Vala M, Barber J, Smith BD, Jones RJ. Anti-tumour activity of interferon alpha in multiple myeloma: role of interleukin 6 and tumor cell differentiation. *Br J Haematol*. 2003;121:251–258.
31. Yang E, Korsmeyer SJ. Molecular thanatopsis: a discourse on the BCL2 family and cell death. *Blood*. 1996;88:386–401.
32. Mejías R, Pérez-Yagüe S, Gutiérrez L, et al. Dimercaptosuccinic acid-coated magnetite nanoparticles for magnetically guided in vivo delivery of interferon gamma for cancer immunotherapy. *Biomaterials*. 2011;32:2938–2952.
33. Jahnke A, Hirschberger J, Fischer C, et al. Intra-tumoral gene delivery of feIL-2, feIFN-gamma and feGM-CSF using magnetofection as a neoadjuvant treatment option for feline fibrosarcomas: a phase-I study. *J Vet Med A Physiol Pathol Clin Med*. 2007;54:599–606.
34. Dou H, Destache CJ, Morehead JR, et al. Development of a macrophage-based nanoparticle platform for antiretroviral drug delivery. *Blood*. 2006; 108:2827–2835.
35. Amendola V, Meneghetti M, Granozzi G, et al. Top-down synthesis of multifunctional iron oxide nanoparticles for macrophage labeling and manipulation. *J Mater Chem*. 2011;21:3803–3813.
36. Carvalho A, Gonçalves MC, Martins MB, Meixedo D, Feio G. Relaxivities of magnetoliposomes: the effect of cholesterol. *Magn Reson Imaging*. 2013;31:610–612.
37. Rudel T. Caspase inhibitors in prevention of apoptosis. *Herz*. 1999; 24:236–241.
38. Hockenbery D, Nuñez G, Milliman C, Schreiber RD, Korsmeyer SJ. Bcl-2 is an inner mitochondrial membrane protein that blocks programmed cell death. *Nature*. 1990;348:334–336.
39. Oltvai ZN, Milliman CL, Korsmeyer SJ. Bcl-2 heterodimerizes in vivo with a conserved homolog, Bax, that accelerates programmed cell death. *Cell*. 1993;74:609–619.
40. Colletier JP, Chaize B, Winterhalter M, Fournier D. Protein encapsulation in liposomes: efficiency depends on interactions between protein and phospholipid bilayer. *BMC Biotechnol*. 2002;2:9.

Supplementary materials

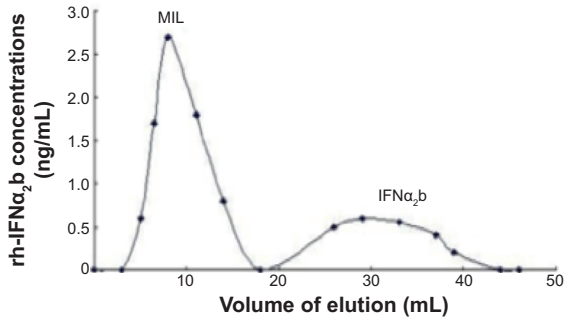

Figure S1 The elution profile shows that magnetoliposomes containing recombinant human (rh)-IFNα_2b (MIL) were purified from the mixture using Sephadex G-50 column chromatography. Two peaks including MIL particles and free IFNα_2b are shown here.

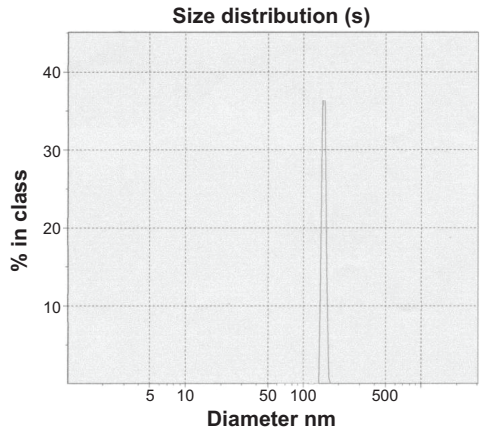

Figure S2 Mean diameters of magnetoliposomes containing recombinant human IFNα_2b (MIL) were determined using dynamic light scattering. As shown, the mean diameter of MIL was approximately 170 nm.

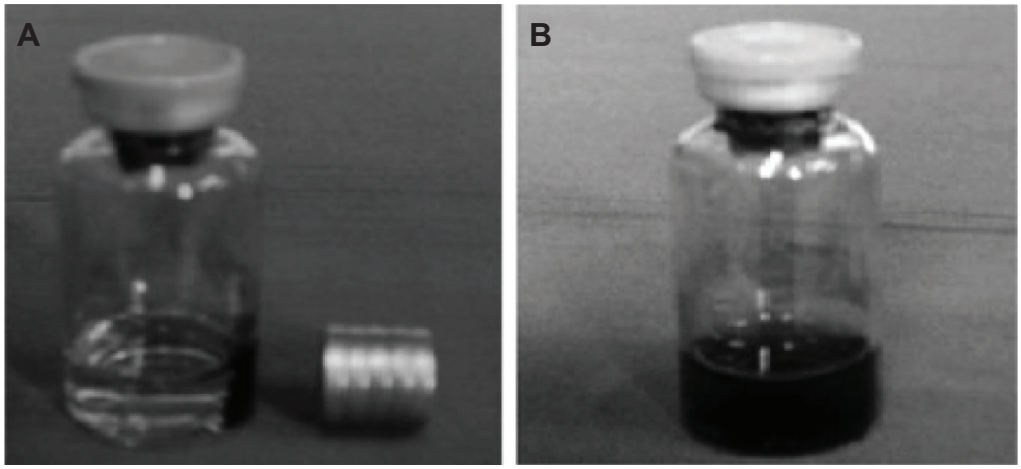

Figure S3 The behavior of magnetoliposomes containing recombinant human IFNα_2b (MIL) in solution with or without an external magnetic field.
Notes: (**A**) MIL was accumulated at one side of the bottle under the external magnetic field. (**B**) MIL was distributed in the solution when no magnet tablet was provided.

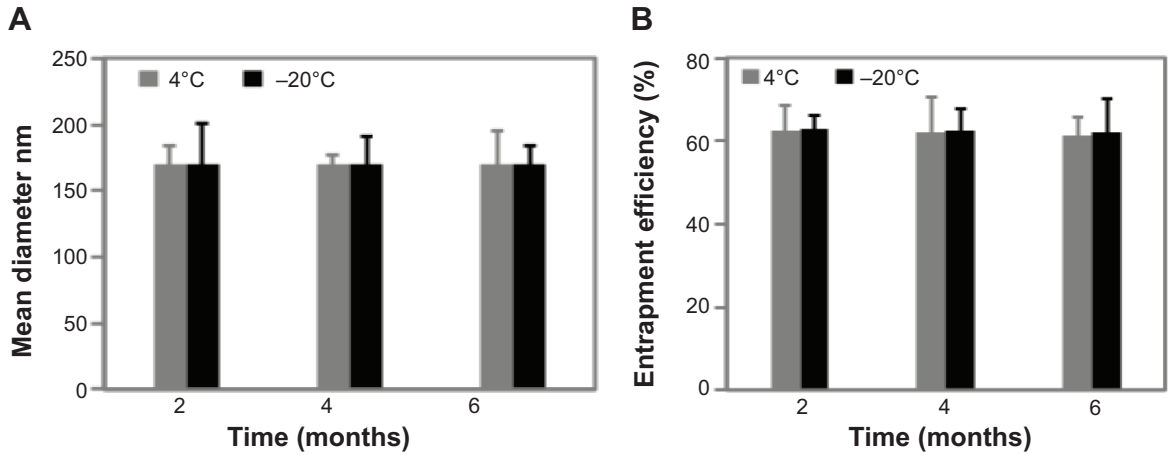

Figure S4 Magnetoliposomes containing recombinant human IFNα_2b (MIL) were stable enough when stored for a long time or at low temperature.
Notes: (**A**) The mean diameter of MIL did not show significant difference when MIL was stored for 6 months at –20°C. (**B**) The drug-entrapment efficiency did not change significantly when MIL was stored for 6 months at –20°C.

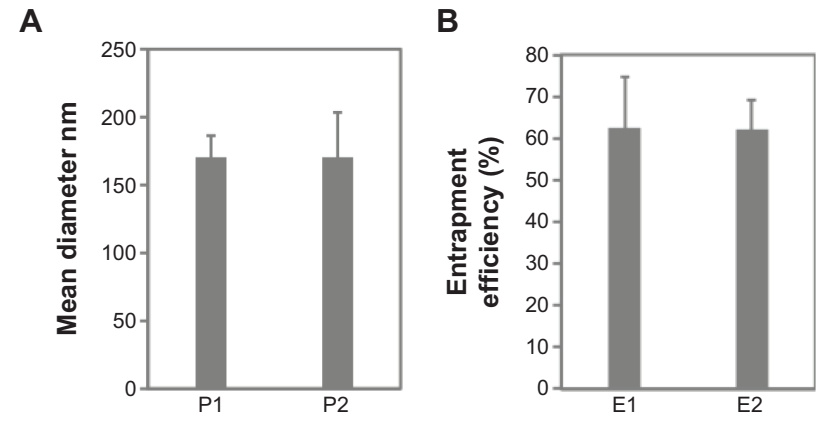

Figure S5 Effect of irradiation sterilization on magnetoliposomes containing recombinant human IFNα2b (MIL).
Notes: (**A**) The mean diameter of MIL particles before and after irradiation sterilization. P1 represents MIL particles before irradiation sterilization, while P2 is the MIL particles after irradiation sterilization. (**B**) Effect of irradiation sterilization on the drug-entrapment efficiency of MIL. E1 is the entrapment efficiency before sterilization, while E2 represents the entrapment efficiency after irradiation sterilization.

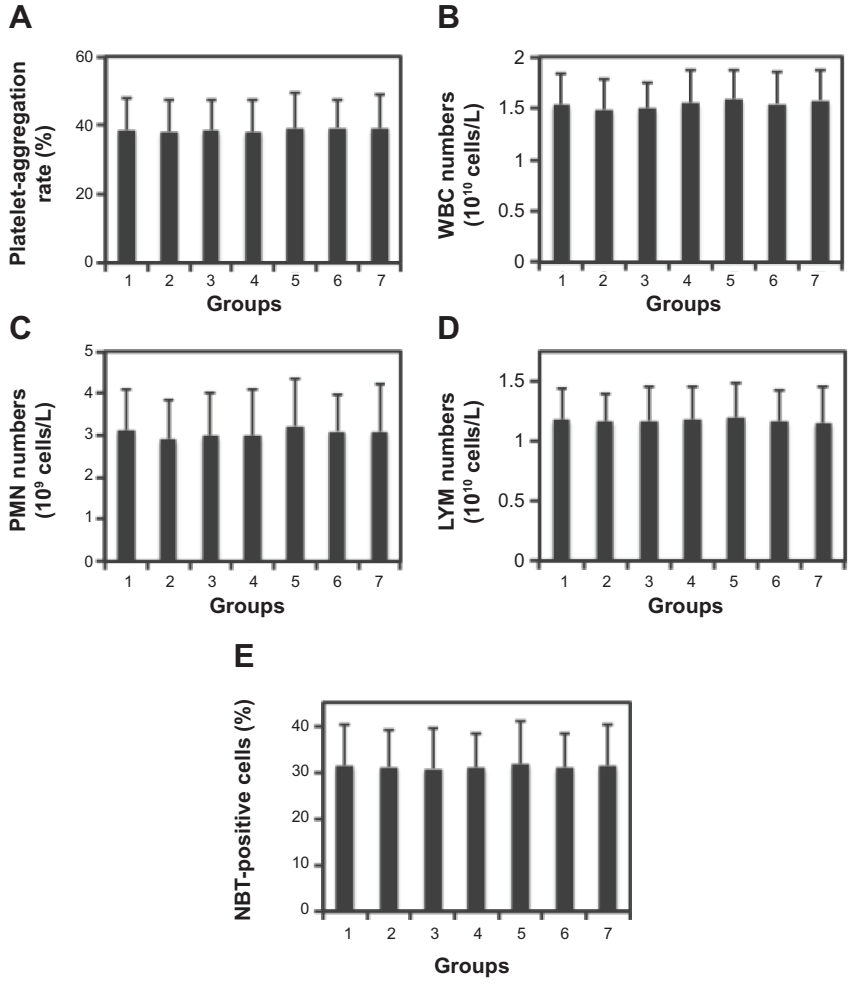

Figure S6 Effects of magnetoliposomes containing recombinant human (rh)-IFNα2b (MIL) on platelets and leukocytes in blood.
Notes: (**A**) Platelet-aggregation rates from seven different groups were shown. Here, group 1 is the control group (NS), in which platelets were treated with saline, whereas groups 2–7 are the platelets treated with MIL containing the following concentrations of rhIFNα2b: 2,000, 4,000, 6,000, 8,000, 10,000, and 12,000 IU/mL. (**B**) Numbers of white blood cells (WBCs) from seven different groups are plotted. The seven groups are as described in **A**. (**C**) Polymorphonuclear leucocytes (PMNs) from the same seven groups are plotted. (**D**) Lymphocytes (LYMs) from the same seven groups are also plotted. (**E**) Nitroblue tetrazolium (NBT)-positive cells were determined using an NBT-reducing test. The results reflect the phagocytic activities of leukocytes in different groups.

Table S1 Observation of animal acute toxicity

Observation item	Signs and symptoms
Spontaneous activity	Increase, decrease, bouncing up and down, lying motionless for reducing tiredness
Muscular movement	Tremor, convulsion, paralysis, ataxia
Muscle tension	Increase, decrease, myotonia, muscle relaxation
Reaction	Nervousness, lags in response
Autonomic nerve movement	Bristling, lacrimation, salivation, exorbitism, diarrhea, writhing reaction
Breathing	Suppression, tachypnea, respiratory failure
Skin color	Pallor, cyanosis, hyperemia
Death time	Sudden death, slow dying
Death symptoms	Struggle, opisthotonos, froth at the mouth

Table S2 Body weights of mice in acute-toxicity test

Group	rhIFNα_2b in MIL (IU)	Numbers of mice	Body weights before administration (g), mean ± SD	Body weights after administration (g), mean ± SD	
				3 days	8 days
Control	0	10	21.03±1.41	21.92±1.73	26.22±1.65
MIL	2×10^6	10	20.79±1.60	21.98±1.58	26.13±0.99
	1×10^6	10	21.11±2.02	22.45±0.89	26.83±1.60
	0.5×10^6	10	20.76±1.68	22.82±1.17	27.01±1.70

Abbreviations: rh, recombinant human; MIL, magnetoliposomes containing rhIFNα_2b; SD, standard deviation.